Published in final edited form as:
Magn Reson Med. 2008 December ; 60(6): 1329–1336. doi:10.1002/mrm.21763.

Improved 3D Phase Contrast MRI with Off-resonance Corrected Dual Echo VIPR

Kevin M Johnson, B.S.[1], **Darren P. Lum, M.D.**[2], **Patrick A. Turski, M.D.**[2], **Walter F. Block, Ph. D.**[1,3], **Charles A. Mistretta, Ph. D.**[1,2], and **Oliver Wieben, Ph.D.**[1,2]

[1]Department of Medical Physics, University of Wisconsin, Madison, WI

[2]Department of Radiology, University of Wisconsin, Madison, WI

[3]Department of Biomedical Engineering, University of Wisconsin, Madison, WI

Abstract

Phase Contrast (PC) magnetic resonance imaging with a three-dimensional, radially undersampled acquisition allows for the acquisition of high resolution angiograms and velocimetry in dramatically reduced scan times. However, such an acquisition is sensitive to blurring and artifacts from off-resonance and trajectory errors. A dual-echo trajectory is proposed with a novel trajectory calibration from prescan data coupled with a multi-frequency reconstruction to correct for these errors. Comparisons of phantom data and in-vivo results from volunteer, and patients with arteriovenous malformations (AVM) patients are presented with and without these corrections and show significant improvement of image quality when both corrections are applied. The results demonstrate significantly improved visualization of vessels, allowing for highly accelerated PC acquisitions without sacrifice in image quality.

Introduction

Volumetric phase contrast (PC) MR imaging with velocity encoding in three spatial dimensions holds the potential to be a comprehensive vascular imaging method; providing both anatomical and quantitative velocity measurements, all without the use of a contrast agent. As a lumenographic imaging tool, it has been effectively used for the identification of aneurysms, arteriovenous malformations (1), and vascular stenoses (2) in the cerebrovascular system, great vessels, and renal arteries. Additional hemodynamic information can be obtained through post-processing of the acquired anatomical and velocity data, providing either velocity visualization and/or quantitative hemodynamic analysis. Visualization of complex velocity fields can be performed by flow vectors, streamlines, and particle traces in order to visually identify pathologic flow patterns (3). Quantitative flow measurements can be accomplished retrospectively with oblique reformats, avoiding difficulties of prospectively targeted 2D PC measurements. Hemodynamic measures such as wall sheer stress and relative pressure can be determined directly from the velocity data (4,5). However, despite the plethora of diagnostic measures available from 3D PC, its clinical use has been hindered by relatively lengthy imaging times and the occurrence of flow related artifacts.

Corresponding Address: Kevin Johnson University of Wisconsin – Madison Department of Radiology J5/M119 Clinical Science Center 600 Highland Avenue Madison, WI 53792-3252 Phone (608) 265-3192 Fax (608) 265-9840 kmjohnson3@wisc.edu .

(Part of this manuscript was presented at the 2007 Annual Meeting of ISMRM, Berlin, Germany)

For 3D PC to become a viable clinical solution, the scan time for images of diagnostic resolution must be reduced. This has been achieved through protocol optimization for vascular territories with larger vessels (6), which usually still results in extended imaging times. Parallel imaging techniques (7,8) can be used in conjunction with optimized protocols, but generally only allow accelerations on the order of 2-4 and can lead to additional SNR degradation. In addition to these accelerated imaging approaches, non-Cartesian trajectories may be used for more efficient sampling schemes, accelerated imaging by undersampling, and the reduction of flow related artifacts.

We have previously introduced Vastly undersampled Isotropic PRojection (VIPR) imaging (9), a 3D radial trajectory with angular undersampling. In PC, we have previously demonstrated that VIPR allowed for high acceleration factors with tolerable undersampling artifacts (10). However, the image quality of PC VIPR acquisitions varied across exams and was frequently compromised by image degradations. In cranial evaluations, PC VIPR images were often found to suffer from incomplete static tissue subtraction, associated undersampling artifacts from un-subtracted tissues, and blurring at the skull base.

Initial investigations identified off-resonance and trajectory errors as the most likely causes of these artifacts, both of which are well documented to cause errors in other non-Cartesian trajectories (11). Off-resonance artifacts can be reduced by shortening the readout window duration; however, this comes at the cost of reduced sampling efficiency, SNR, and increased error from trajectory deviations. Likewise, trajectory errors can be reduced by reducing the readout gradient strength, as trajectory errors scale with the gradient amplitude (14); however this leads to blurring and signal cancellations from T2* and off-resonance. In this study we investigated data inconsistencies in PC VIPR imaging and propose adjustments in the acquisition and reconstruction to correct off-resonance and trajectory errors, significantly improving image quality and the acquisition efficiency. These improvements in consistency and performance of are demonstrated on ungated PC VIPR exams, but are extendable to general 2D and 3D PC sequences.

Materials and Methods

Off-Resonance Corrections

Spatially dependent off-resonance changes the encoding basis functions to a non-Fourier set. Therefore, errors ensue when data is reconstructed assuming Fourier encoding. In Cartesian imaging the effect of off-resonance is limited as errors only occur along the readout direction; however; during a 3D radial acquisition all three spatial encoding directions are performed using readout gradients, leading to errors in all three directions. With a known off-resonance map, the basis set is known, allowing non-Fourier reconstruction using iterative least squares minimization (12). Unfortunately, this generally results in extended reconstruction times. In the case of a smoothly varying field map (e.g. the field map gradient is small with respect to the encoding), accurate reconstructions can be obtained with the multi-frequency reconstructions (13). This requires the reconstruction of each data set at several different frequencies which are interpolated to find the final image. With T2* decay of blood limiting the readout length and subsequently limiting errors from spatial field map variations, multi frequency reconstructions are well suited for the readouts associated with PC VIPR.

Trajectory Corrections

While a number of methods exist for measuring and correcting trajectories, the approach proposed by Duyn et. al. (14) has become a popular choice for its accuracy without need for specialized phantoms . For most sequences, the trajectory measurements can be derived

using this method only along the three physical gradients while all other encoding steps are assumed to be a linear combination of these gradients (15). This is possible because the waveforms on any given axis are scaled versions of the reference waveform. However due to the bipolar gradient pair required for velocity encoding, the gradient waveforms played in a single TR for PC are not a simple linear combination of the trajectory along the three physical axes, but rather a combination of several waveforms per axis. Thus, without further simplification, measurements would need to be measured for all projections angles with each of the four flow encoding gradients making per-scan calibrations impractical. Trajectory measurements, however, can be simplified if we assume the gradient deviations to be the result of a linear operator. This requires us to expand the previous assumptions of homogeneity to include superposition of each gradient. Homogeneity corresponds to scaling linearity, (e.g. double the gradient amplitude double the gradient error). Superposition implies that applying two gradients independently and adding the errors results in the same errors as applying the gradients together. If this can be assumed, the trajectory can be represented as a sum of the deviations from each gradient trapezoid:

$$\Delta k = \sum_{i=0}^{N} a_i \Delta k_i$$

Where N is the total number of independent gradient waveforms, a_i is the relative amplitude of the i^{th} gradient waveform, Δk_i is the measured trajectory of the i^{th} gradient waveform, and Δk is the total deviation expressed as k-space sampling points. For a standard PC exam, this approach requires four measurements for each axis (no gradient, first lobe of bipolar, second lobe of bipolar, and readout) in comparison to two measurements per axis (no gradient, prewinder+readout) required for non-PC sequences.

Dual-Echo Readout

The capabilities for off-resonance and trajectory corrections allows for more flexibility with the k-space trajectories without dramatic losses in image quality. In particular, it enables multi-echo acquisitions, which in turn are capable of producing the off-resonance map used for corrections. Without off-resonance corrections, long durations between successive echoes cause phase incoherence resulting in signal loss at areas with off-resonances. While this property can be exploited for the separation of fat and water (16), it is prohibitive in PC VIPR imaging because of the signal loss. Without gradient calibration techniques to compensate for trajectory errors, the resulting phase errors between the echoes cause inaccuracies in the field maps and signal cancellation in images.

Previous implementations of multi-echo VIPR (16,17) are well suited for general gradient echo imaging, but due to poor k-space symmetry of each echo and 1^{st} moment trajectory are ill suited for radial phase contrast MRI. Figure 1 shows a modified dual-echo VIPR trajectory designed to optimize the acquisition for phase contrast imaging. The corresponding 0^{th} and 1^{st} moment trajectories shown in Figure 2. Two fractional echoes are acquired in each TR with the distance between the echoes times minimized. The data sampling window extends from the start of the first readout gradient to the end of the second readout gradient, covering gradient ramps and the ‘blip’ when transitioning from the first to the second echo; however data collected during the ‘blips’ is not used for the reconstruction. Flow compensation is achieved by first moments of both echoes that are aimed to offset each other. Velocity encoding gradients are played out in all three directions for all four encodings, using TE minimized calculations (18) and a gradient balanced 4-point encoding scheme (19). The use of gradient balanced encoding reduces the required gradient areas and, thereby, leads to shorter echo times and reduced velocity dispersion related dephasing

effects; which counterbalance the incomplete flow compensation. The flow compensation method itself also reduces the required size of the bipolar gradients leading to even shorter TEs.

Gradient Linearity Validation

All measurements were performed on clinical 3.0 T system (HD EXCITE TwinSpeed Signa, GE Healthcare, Waukesha, WI; slew rate: 80 mT/m/ms, max gradient strength: 40 mT/m). Initial tests were performed to determine whether the assumption of gradient linearity was valid for PC VIPR imaging. This experiment was tailored mainly to test superposition, as homogeneity scaling has been previously demonstrated (15) . Therefore, the pulse sequence was modified to perform a linear system test:

$$G(aA+bB)=aG(A)+bG(B),$$

where G is the gradient deviation operator, A and B are trapezoidal pulses, and a and b are scaling factors. Gradient deviation measurements were made with A alone, B alone, and both, A and B, applied. The summation of the deviations measured when pulses A and B were played out individually was compared to the actually measured trajectory when both gradients were applied simultaneously. This test was performed over the range of bipolar amplitudes and pulse widths typically used in PC VIPR. For phase contrast imaging, the bipolar gradients are almost always initially played out at their maximum amplitude, due to first moment requirements for flow compensation and velocity encoding. Thus, all ramp widths were set to the rise time of the system (244 μs). The amplitude and width of trapezoid A was fixed, with a 300 μs plateau and maximum amplitude of 36 mT/m. The amplitude and pulse width are typical and were chosen specifically to ensure eddy currents representative of an actual acquisition. The amplitude of B was measured at the two extremes of +36 mT/m and −36 mT/m at plateau pulse widths of 100, 200, and 300 μs. The acquisition window extends from 50 μs before the first pulse to 1000 μs after the end of the second pulse, thereby covering any major persistent effects.

Sequence Evaluation

Phantom, volunteer, and patient studies were performed to assess the efficacy of corrections and image quality. Data were acquired covering a 22×22×22 cm^3 field of view with 0.6 mm isotropic resolution (nominal). A 75% fractional echo was used with a 62.50 kHz readout and 125 kHz receiver bandwidth. The velocity encoding (VENC) was set to 60 cm/s, resulting in a TR of 11.6 ms and TE's of 3.5 and 6.1ms. A 15° flip angle was used in all cases, chosen based on empirical observations to minimize signal saturation. A total of 14,000 projections (28000 TRs) were collected for a total scan time of 5:24 minutes, representing an under sampling factor of 11 with respect to Nyquist. Trajectory calibrations were performed using 16 averages per direction with a 15° flip angle and a 40 ms TR; adding an additional 23 s to the exams. For all experiments an 8 channel phased array head coil was used for acquisition (HD Brain Coil, GE Healthcare, Milwaukee, WI). All reconstructions were performed using an optimized gridding operation (20) with conjugate phase reconstruction performed using least squares interpolations of 7 evenly spaced frequencies (21). Off-resonance maps were created using low-resolution phase images between echoes, with phase aliasing removed using a simple region growing algorithm. From the reconstructed velocity and magnitude images, an angiographic image was created using:

$$CD = \begin{cases} M \cdot \sin\left(\frac{\pi}{2} \cdot |\vec{V}|/V_A\right) & |\vec{V}| < V_A \\ M & \text{otherwise} \end{cases}$$

Where CD is the angiographic image, M is the magnitude, $\vec{V}$ is the velocity as determined from phase processing, and V_A is an arbitrarily defined threshold velocity. This weighting scheme mimics complex difference processing (22), but allows use of balanced 4-point imaging and phase difference processing. For all reconstructed images reported here, V_A was set to the VENC of 60 cm/s.

A standard quality assurance phantom was imaged for the evaluation of off-resonance and trajectory corrections. Magnitude phantom images were reconstructed without off-resonance or trajectory corrections, with off-resonance corrections, with trajectory corrections, and with both trajectory and off-resonance corrections. These images were then qualitatively evaluated for image distortions and artifacts as compared to the known geometry.

Subsequently, five normal volunteers and five patients with known arteriovenous malformations (AVM) were examined with institutional board approval and informed patient consent for an in-vivo assessment of the extended PC VIPR acquisition technique. Image quality comparisons were made, examining background suppression, edge sharpness and vessel visualization, between corrected (off-resonance + trajectory) and uncorrected angiographic images by 2 board certified, blinded readers, with criteria defined in Table 1. Edge sharpness and background suppression were evaluated over the entire volume, while vessel visualization was evaluated individually on the carotids, middle cerebral arteries (MCA), anterior cerebral/communication arteries (ACA/ACOMM), vertebral (VERT), and posterior cerebral arties (PCA). Statistical significance of differences in scores was determined using a Friedman test (n=5) for each category and across observers using both patient an volunteer populations. The significance image quality differences between volunteer and patient populations were determined using a Friedman test (n=5) of corrected images, across all categories.

Results

Trajectory Correction Linearity

The root mean square (RMS) trajectory difference between the combined gradients and the combined trajectories was measured for each gradient combination and gradient direction. The maximum RMS error, expressed in k-space points for a 22 cm FOV, along the left-right (L/R), anterior-posterior (A/P), and superior-inferior (S/I) directions was determined to be 0.0039, 0.0026, and 0.0020 points respectively, compared to a maximum deviation of ~1.0 k-space points. Figure 3, shows representative deviations for the L/R gradient coil with a gradient B pulse width of 100 μs and amplitude of −36 mT/m. Uncompensated eddy currents extend well beyond each of the pulses on this particular gradient coil. The gradient area is relatively accurate with the deviation approaching zero after decay. The A/P coil has a similar eddy current pattern, while the S/I coil has a rapid decay of eddy currents and reduced deviations on average.

Phantom Studies

Representative mid-slab axial images of the phantom are shown in Figure 4. Images with no corrections (A), show signal distortion manifesting as blurring and focal areas of signal loss. Images with trajectory corrections only (B) show improved image quality by reducing the artifact to a symmetric blurring, which is the expected behavior for off-resonance. Images

with off resonance correction only (C) show some improvement but the non-symmetric blurring from the trajectory errors remains. Only if both corrections are applied (D), images of high quality are reconstructed and appear free of artifacts.

Human Studies

Exams of all volunteers and patients were successfully acquired, yielding images of diagnostic quality. Compared to the image quality in previously reported work (10), images demonstrate dramatic improvement. Figure 5 shows representative full FOV maximum intensity projection (MIP) images from a volunteer exam. The images show excellent background suppression and vessel delineaton across the entire FOV. Vascular structures as small as 1.5-2.0 mm are easily identified, including those of the temporal arteries. Figure 6 shows representative limited MIP images from volunteers exams reconstructed with no corrections, with off-resonance corrections alone, and with both off-resonance and trajectory corrections. Without any corrections significant blurring and focal areas of signal loss are seen above the paranasal sinuses. While off-resonance corrections help to eliminate phase cancellations, significant blurring remains which is only removed when both, off-resonance and trajectory corrections, are applied. Representative patient images are shown in Figure 7, showing excellent visualization of the feeding arteries/veins and nidus. Blinded reader evaluations are shown in Table 2. Image quality significantly improves in all aspects when the corrections are applied. Statistical tests show a significant difference between corrected and uncorrected images in all three categories ($P<0.005$), and no statistically significant differences between observers ($P=0.64$) and patient/volunteer image quality ($P=0.44$).

Discussion

The clinical use of Non-Cartesian imaging is largely inhibited by image degradation either inherent to the trajectory itself or due to physical inaccuracies in the acquisition. The extent to which these imperfections affect the image quality is dependent on the acquisition and trajectory used. Proper treatment of errors associated with the Non-Cartesian trajectory can reduce these trajectory based dependencies, allowing trajectories tailored to the application. PC VIPR is particularly sensitive to a wide variety of image degradations, accumulating both the errors associated with phase contrast and Non-Cartesian trajectories. Dual-echo PC VIPR is a self contained solution to address both, off-resonance and trajectories errors, with the added benefit of reducing eddy-current errors that generally causes errors in phase contrast velocimetry.

The corrections are effective in improving image quality, both in phantom experiments and invivo in patients and volunteers. These findings indicate that errors from off-resonance and trajectory errors can significantly degrade image quality in non-Cartesian phase contrast MRI. The extent of the error is likely to be highly dependent both on the gradient coil system of the scanner and the region of interest. Off-resonance errors are likely to be reduced in areas of homogenous susceptibility, such as the thighs an pelvis; and conversely, much worse in areas of heterogeneous susceptibility, as in the chest. As long as an off-resonance map can be determined, these errors should be correctable. In this work, the off-resonance map was determined from the dual echo trajectory itself, eliminating the need for a separate co-registered map. Using this approach in other vascular regions will be more difficult, as the map will be corrupted by fat signal. This may force the use of separate chemical shift sequences (23) in such regions.

The dual-echo PC VIPR sequence, with all corrections applied, is a significant improvement over the initially reported single echo, uncorrected implementation (10); which was itself a significant improvement over 3D Cartesian phase contrast sequences for accelerated imaging. In reference to the original PC VIPR implementation, the dual echo sequence has

shorter TE's and TR's both from the change to a balanced encoding scheme and from a much higher readout bandwidth. This high readout bandwidth is possible due to the dual-echo sampling and the signal gain from the higher magnetic field (3T vs. 1.5T). Unlike TOF imaging, PC protocols do not require lengthy TR's and the flip angle can be adjusted to maximize signal at any TR. Shorter TR's allow more projections to be acquired in a given time, reducing artifact from undersampling, overcoming SNR loss from shorter TR's. Thus when compared to the previous version, the dual echo PC VIPR sequence has much lower undersampling ratios in the same scan time, with improved image quality even without any corrections.

Future work is required to evaluate the efficacy of corrections on quantitative velocity information and compare the proposed method to other techniques. No investigation has been performed on the possible influence of corrections on the velocity measurements. Since the angiographic data used for evaluation is based on velocity data, it is likely that the improvements in image quality, background suppression, and sharpness extend to the velocity data. Of particular interest will be the influence of corrections on background phase offsets which can lead to significant errors in flow measurements(24). Furthermore, investigations in this paper were limited to the dual-echo VIPR trajectory. It is likely that other trajectories will benefit from off-resonance and trajectory corrections. Eddy current corrections will reduce velocity offset errors in all sequences, especially in short TE sequences where eddy currents from the bipolar will not have time to decay away. Other Non-Cartesian trajectories, such as spiral (25) will show improvements in spatial response from both off-resonance and trajectory corrections.

The dual-echo PC VIPR sequence represents a significant advancement in PC angiography and velocimetry. With the sequence, PC imaging can be performed at high spatial resolution with excellent background subtraction covering a large imaging volume. It provides a viable alternative for non-contrast-enhanced MRA (CE-MRA) imaging in areas or patients where TOF and CE-MRA is not possible, of poor quality, or too time-consuming. This may prove especially powerful in patients at risk of Nephrogenic Systemic Fibrosis (26) or other cases where gadolium based contrast agents are not tolerated. In those patients where the use of contrast agents is acceptable, PC imaging may provide complementary anatomical information with the superior spatial resolution compared to a bolus chase technique. In addition, PC VIPR provides functional information in form of velocity vector fields with spatial and temporal resolutions not generally feasible with standard Cartesian sequences due to extended imaging times. The availability of anatomical and functional information allows for the analysis of hemodynamic relevant parameters such as velocity patterns and flow, pressure gradients, and wall shear stress. With a better understanding of the relevance of these parameters to disease processes, patient care could possibly improve significantly with patient specific, non-invasive measures e.g. for vascular remodeling processes, likelihood for ruptures of aneurysms, and others.

Conclusion

In this study, we have developed a novel, radial 3D PC sequence capable of acquiring high-resolution whole brain, angiographic images in clinically feasible scan times. Utilizing central k-space oversampling, self calibrated corrections were devised to correct for spatial distortions caused by off-resonance. Additionally a short prescan method was developed to measure trajectory deviations from eddy currents and timing errors. In phantoms, volunteers, and patients images were compared with and without corrections for off-resonance and trajectory errors. From this comparison, it follows that the combination of both corrections leads to significant improvements in image quality, reducing artifacts from susceptibility and eddy currents.

Acknowledgments

This work was supported by NIH grant 1RO1-HL62465.

References

1. Huston J, Rufenacht DA, Ehman RL, Wiebers DO. Imtracranial Aneurysms and Vascular Malformations: Comparison of Time-of-Flight and Phase-Contrast Angiography. Radiology. 1991; 181(3):721–730. [PubMed: 1947088]
2. Oelerich M, Lentschig MG, Zunker P, Reimer P, Rummeney EJ, Schuierer G. Intracranial vascular stenosis and occlusion: comparison of 3D time-of-flight and 3D phase-contrast MR angiography. Nueroradiology. 1998; 40(9):567–573.
3. Markl M, Draney MT, Miller DC, Levin JM, Williamson EE, Pelc NJ, Liang DH, Herfkens RJ. Time-resolved three-dimensional magnetic resonance velocity mapping of aortic flow in healthy volunteers and patients after valve-sparing aortic root replacement. J Thorac Cardiovasc Surg. 2005; 130(2):456–463. [PubMed: 16077413]
4. Tyszka JM, Laidlaw DH, Asa JW, Silverman JM. Three-dimensional, time-resolved (4D) relative pressure mapping using magnetic resonance imaging. J Magn Reson Imaging. 2000; 12(2):321–329. [PubMed: 10931596]
5. Papathanasopoulou P, Zhao S, Kohler U, Robertson MB, Long Q, Hoskins P, Xu XY, Marshall I. MRI measurement of time-resolved wall shear stress vectors in a carotid bifurcation model, and comparison with CFD predictions. J Magn Reson Imaging. 2002; 17(2):153–162. [PubMed: 12541221]
6. Markl M, Chan FP, Alley MT, Wedding KL, Draney MT, Elkins CJ, Parker DW, Wicker R, Taylor CA, Herfkens RJ, Pelc NJ. Time-resolved three-dimensional phase-contrast MRI. J Magn Reson Imaging. 2003; 17(4):499–506. [PubMed: 12655592]
7. Pruessmann KP, Weiger M, Scheidegger MB, Boesiger P. SENSE: sensitivity encoding for fast MRI. Magn Reson Med. 1999; 42(5):952–962. [PubMed: 10542355]
8. Sodickson DK, Manning WJ. Simultaneous acquisition of spatial harmonics (SMASH): fast imaging with radiofrequency coil arrays. Magn Reson Med. 1997; 38(4):591–603. [PubMed: 9324327]
9. Barger AV, Block WF, Toropov Y, Grist TM, Mistretta CA. Time-resolved contrast-enhanced imaging with isotropic resolution and broad coverage using an undersampled 3D projection trajectory. Magn Reson Med. 2002; 48(2):297–305. [PubMed: 12210938]
10. Gu T, Korosec FR, Block WF, Fain SB, Turk Q, Lum D, Zhou Y, Grist TM, Haughton V, Mistretta CA. PC VIPR: a high-speed 3D phase-contrast method for flow quantification and high-resolution angiography. Am J Neuroradiol. 2005; 26(4):743–749. [PubMed: 15814915]
11. Noll DC, Pauly JM, Meyer CH, Nishimura DG, Macovski A. Deblurring for non-2D Fourier transform magnetic resonance imaging. Magnetic Resonance in Medicine. 1992; 25(2):319–333. [PubMed: 1614315]
12. Fessler JA, Lee S, Olafsson VT, Shi HR, Noll DC. Toeplitz-based iterative image reconstruction for MRI with correction for magnetic field inhomogeneity. IEEE Trans Sig Proc. 2005; 53(9): 3393–3402.
13. Noll DC, Meyer CH, Pauly JM, Nishimura DG, Macovski A. A Homogeneity Correction Method for Magnetic-Resonance-Imaging with Time-Varying Gradients. Ieee Transactions on Medical Imaging. 1991; 10(4):629–637. [PubMed: 18222870]
14. Duyn JH, Yang YH, Frank JA, van der Veen JW. Simple correction method for k-space trajectory deviations in MRI. Journal of Magnetic Resonance. 1998; 132(1):150–153. [PubMed: 9615415]
15. Lu A, Brodsky E, Grist TM, Block W. Rapid Fat-Suppressed Isotropic Steady-State Free Precession Using True 3D Multiple-Half-Echo Projection Reconstruction. Magn Reson Med. 2005; 53:692–699. [PubMed: 15723411]
16. Lu A, Grist TM, Block W. Fat/water separation in single acquisition steady-state free precession using multiple echo radial trajectories. Magn Reson Med. 2005; 54(5):1051–1057. [PubMed: 16217786]

17. Liu J, Redmond MJ, Brodsky EK, Alexander AL, Lu A, Thornton FJ, Schulte MJ, Grist TM, Pipe JG, Block WF. Generation and visualization of four-dimensional MR angiography data using an undersampled 3-D projection trajectory. IEEE Trans Med Imaging. 2006; 25(2):148–157. [PubMed: 16468449]

18. Bernstein MA, Shimakawa A, Pelc NJ. Minimizing TE in moment-nulled or flow-encoded two- and three-dimensional gradient-echo imaging. Journal of Magnetic Resonance Imaging. 1992; 2(5):583–588. [PubMed: 1392252]

19. Pelc NJ, Bernstein MA, Shimakawa A, Glover GH. Encoding strategies for three-direction phase-contrast MR imaging of flow. J Magn Reson Imaging. 1991; 1(4):405–413. [PubMed: 1790362]

20. Beatty PJ, Nishimura DG, Pauly JM. Rapid gridding reconstruction with a minimal oversampling ratio. IEEE Trans Med Imaging. 2005; 24(6):799–808. [PubMed: 15959939]

21. Man LC, Pauly JM, Macovski A. Multifrequency Interpolation for Fast Off-resonance Correction. Magn Reson Med. 1997; 37(5):785–792. [PubMed: 9126954]

22. Bernstein MA, Ikezaki Y. Comparison of phase-difference and complex-difference processing in phase-contrast MR angiography. Journal of Magnetic Resonance Imaging. 1991; 1(6):725–729. [PubMed: 1823179]

23. Reeder SB, Wen Z, Yu H, Pineda AR, Gold GE, Markl M, Pelc NJ. Multicoil Dixon chemical species separation with an iterative least-squares estimation method. Magn Reson Med. 2004; 51(1):35–45. [PubMed: 14705043]

24. Chernobelsky A, Shubayev O, Comeau CR, Wolff SD. Baseline Correction of Phase Contrast Images Improves Quantification of Blood Flow in the Great Vessels. Journal of Cardiovascular Magnetic Resonance. 2007; 9(4):681–685. [PubMed: 17578724]

25. G. Bruce Pike CHMTJBNJP. Magnetic resonance velocity imaging using a fast spiral phase contrast sequence. Magnetic Resonance in Medicine. 1994; 32(4):476–483. [PubMed: 7997113]

26. Thomsen HS, Morcos SK, Dawson P. Is there a causal relation between the administration of gadolinium based contrast media and the development of nephrogenic systemic fibrosis (NSF)? Clinical Radiology. 2006; 61(11):905–906. [PubMed: 17018301]

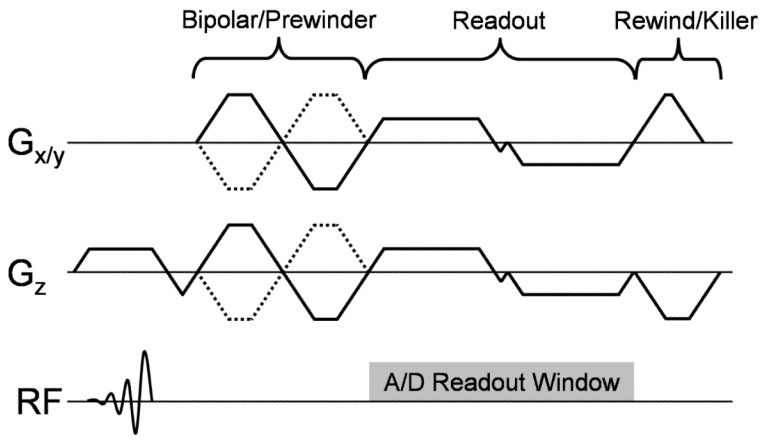

Figure 1.
Pulse sequence diagram for dual-echo PC VIPR, consisting of a combined bipolar/prewinder, dual-echo readout, and gradient rewinders and spoilers. Gradient spoiling is applied consistently on the z-gradient with x and y gradients are rewound back to the center of k-space.

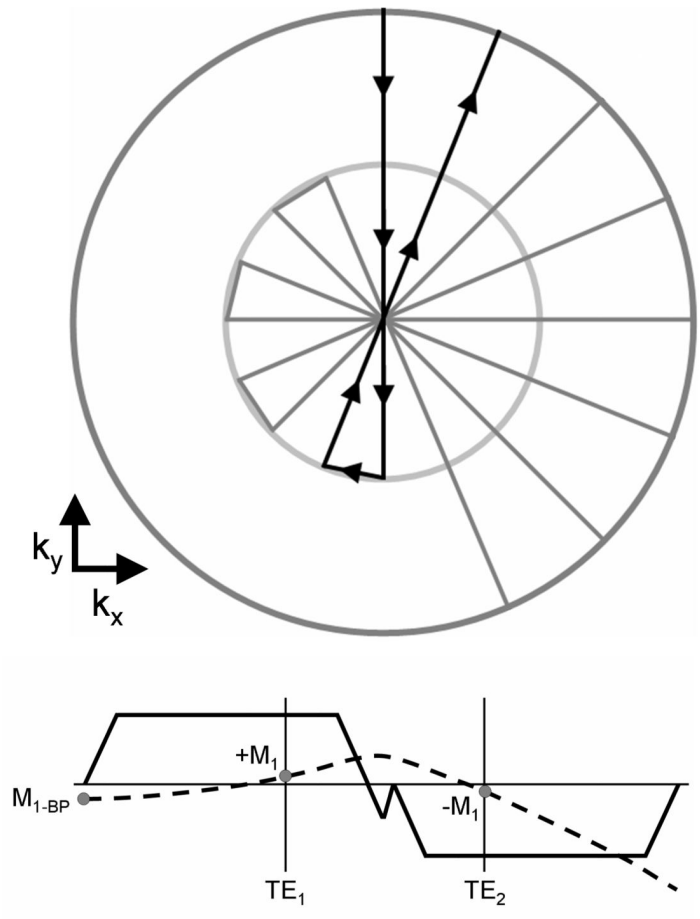

Figure 2.
Zeroeth (top) and first (bottom) moment trajectory of the dual echo readout. The 0^{th} moment trajectory, show along starts at the edge of k-space, passes through the center, changes angles and proceeds back to the edge of k-space. The 1^{st} moment of this trajectory, shown applied along the k_r (projection) direction, is flow compensated with first moments equally minimized.

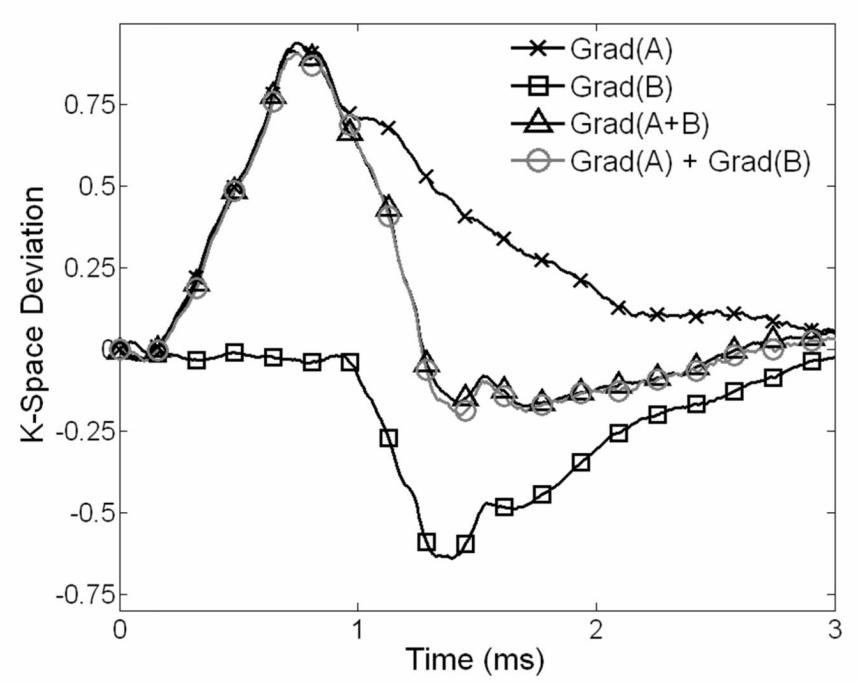

Figure 3.
Comparison of trajectory deviations along the x-axis when two trapezoid gradients are played (1) together within one acquisition and (2) individually in two successive acquisitions. The system is well approximated with linear assumptions, shown by the agreement between the calculated deviation by adding gradients A and B and that actually measured with both gradients on.

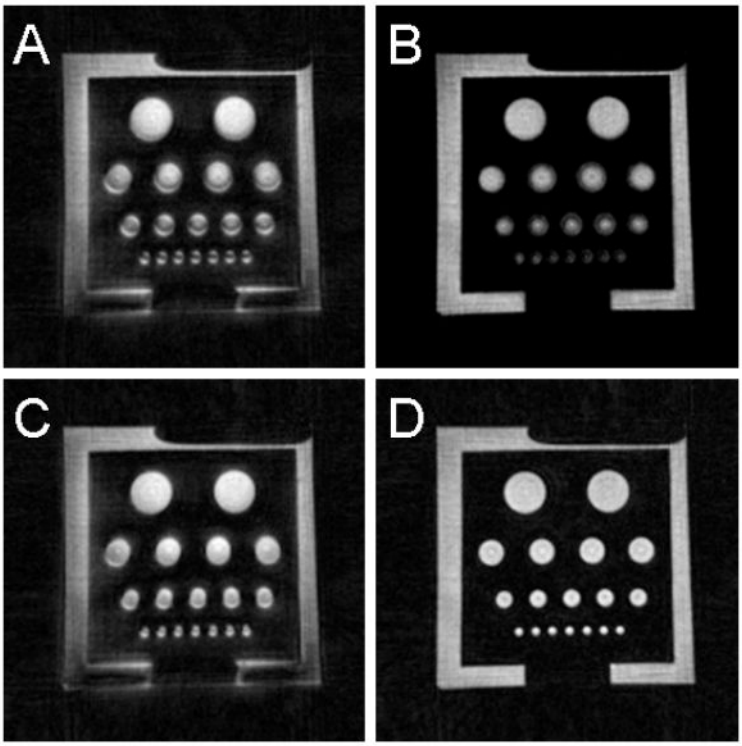

Figure 4.
Magnitude images of a phantom: uncorrected (A), trajectory corrected (B), off-resonance corrected (C), and with both corrections (D). Neither trajectory nor off-resonance corrections alone where successful in producing a high quality image, however, when both correction schemes are applied the image quality is significantly improved.

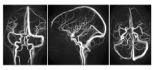

Figure 5.
Representative coronal, sagittal, and axial full volume MIP images from a cranial PC VIPR exam, demonstrating the extensive coverage and excellent spatial resolution. Small arteries are well visualized with almost complete background subtraction.

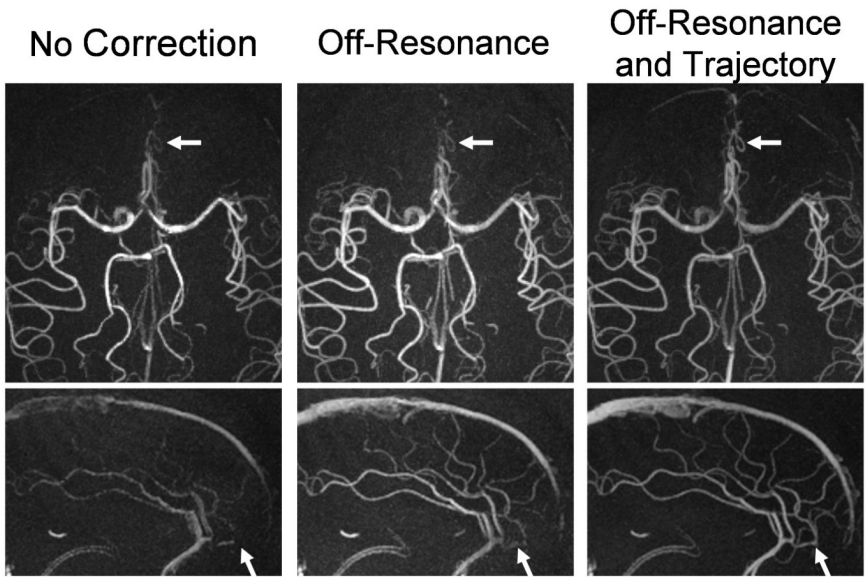

Figure 6.
Limited axial and sagittal MIP images from a cranial PC VIPR exam with no corrections (left), with off-resonance corrections alone (middle), and with both off-resonance and trajectory corrections (right). Only when all corrections are applied do images show clear delineation of small vessels above the nasal cavity.

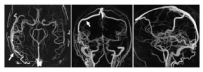

Figure 7.
Limited axial(left), coronal(middle), and sagittal(right) mips of a patient with an AVM in the anterior left lobe. Images show excellent delineation of both the feeding arteries/veins and nidus. Arrows point to a the nidus (left) and main draining vein (middle).

Table 1

Scoring guidelines used by two blinded readers.

Category	Description	Score
Background	Substantial background that interferes with diagnostic interpretation.	0
	Moderate background signal, does not interfere with interpretation.	1
	No Substantial Noise (i.e. very good background subtraction)	2
Blurring/Edge Sharpness	Severe Blurring. Vessel dropouts. Non-diagnostic.	0
	Moderate to Severe blurring. Loss of Diagnostic Accuracy.	1
	Moderate blurring. Does not interfere with diagnostic interpretation.	2
	Minimal blurring.	3
	No evident blurring.	4
Vessel Visualization	*Non-Diagnostic or Not Visible*	0
	Poor (Structures visible but with significant blurring or artifacts, barely diagnostic)	1
	Fair (Anatomy visible, moderate blurring or artifacts, partially diagnostic)	2
	Good (Good quality diagnostic information, minimal blurring or artifacts)	3
	Excellent (Excellent quality diagnostic information, sharply defined borders)	4

Table 2

Median result from radiologist evaluation (observer 1/observer 2). With corrections, image quality is substantially improved in all vessels/aspects (P<0.005). Scoring guidelines are outlined in Table 1.

		Background Blurring		Vessel Visualization					
		Overall (0-2)	**Overall (0-4)**	**Overall (0-4)**	**Carotids (0-4)**	**MCA (0-4)**	**ACA/ACOMM (0-4)**	**VERT (0-4)**	**PCA (0-4)**
Patients	Corrected	2/1	3/1	4/3	3/3	3/3	3/3	3/3	4/3
	w/o Corrections	1/0	0/1	0/1	0/1	0/1	0/1	0/1	0/1
Volunteers	Corrected	2/1	4/3	4/4	4/4	4/4	4/4	4/4	4/4
	w/o Corrections	1/0	1/2	1/2	0/2	2/2	0/2	2/2	2/2